Reconstruction from voxel objects with guarantees
Supplementary material

David Coeurjolly, Jacques-Olivier Lachaud and Pierre Gueth

CONTENTS

1 SHORT DESCRIPTION OF OUR SHROUDS IMPLEMENTATION

We present briefly our implementation of the "Shrouds" method [1], since no code was publicly available. First, the method is presented in a rather informal manner, but digital topology results [2], [3] back up the fact that their 4^*-network obtained by slicing is a separating manifold: it is indeed the (bel) adjacency graph of the digital surface that borders the set of voxels, for some choices of connectivity between voxels. Second, the problem of minimizing the squared curvature under hard constraint is not convex and one must be careful at how to process in its numerical approximation. Then the paper is rather unclear at how each individual contour is optimized (according to either squared curvature or just second order penalty), with either "a parametric quadratic polynomial" joining previous and next vertices or "a cubic spline [. . .] at some additional computational cost". Note that the first approach does not work out as is since it puts each vertex on the line segment joining its two neighbors and the process does not converge. Last, the paper does not say how results on different slices are combined.

Our approach is to optimize each vertex along its two intersecting slices. The process alternates a step where we compute the distance between vertices along slices (i.e. estimation of a correct parameterization), and a step where each vertex is moved along its edge in order to minimize the local squared curvature along both slices. More precisely, for some vertex v_i along some slice, let (x_i, y_i) be its 2D coordinates. This vertex is forced to stay on a unit edge between an inner voxel p_i and an outer voxel q_i, so we associate a parameter $t_i \in [\epsilon, 1-\epsilon]$ to this vertex, and $(x_i, y_i) = (1-t_i)p_i + t_i q_i$.

Euler-Lagrange equations for minimizing squared curvature give the following necessary conditions at equilibrium (using prime to denote the derivation with respect to a parameterization t of contour $(x(t), y(t))$:

$$
\begin{aligned}
0 =& 24x'^3x''^3y' + x'''(-13x'^4x''y' - 14x'^2x''y'^3 - x''y'^5) \\
&+ x''''(x'^5y' + 2x'^3y'^3 + x'y'^5) \\
&+ y'''(8x'^5x'' + 4x'^3x''y'^2 - 4x'x''y'^4) \\
&+ y''(12x'^4y'y''' + 12x'^2y'^3y''' - 24x'^4x''^2 + 5x'^5x''') \\
&+ y''(51x'^2x''^2y'^2 - 2x'^3x'''y'^2 + 3x''^2y'^4 - 7x'x'''y'^4) \\
&+ y''^2(-54x'^3x''y' + 18x'x''y'^3) \\
&+ y''^3(3x'^4 - 21x'^2y'^2) \\
&+ y''''(-x'^6 - 2x'^4y'^2 - x'^2y'^4)
\end{aligned}
$$

At any vertex, either x_i or y_i is fixed and does not depend on t_i. For instance, if we assume x_i is fixed, the two first lines do not depend on t_i. For y''' we use the approximation at preceding time step. x' and y' are estimated with centered finite

difference so do not depend on t_i. Terms y''^2 and y''^3 are linearized as $y''y''_{old}$ and $y''y''^2_{old}$. Term y'''' is approximated with centered finite difference with again the unknwon y'' and y''_{old} at next and previous positions. Gathering all, we get an expression of the form $\alpha_i y''_i = \beta_i$ for each direction, that we sum. Finally, term y''_i is approximated with centered finite differences so that optimal parameter t_i for y_i is found.

Since the energy is not convex, we perform a damped gradient descent and we stop after 1000 iterations. Although this algorithm generally does not converge (displacement norm stays greater than 0.01), it gives nice results visually.

2 Experimental stability of the regularization

First of all, we illustrate the robustness to noise of our approach. In Figure 1, we have added random perturbations of different magnitude to the normal vectors used in (a). For some extreme noise (0.5 and 0.8 shifts), the geometry is highly distorted but the overall shape is still consistent. For application specific regularization, adjusting the alignment term coefficient β can handle such high noise levels. (Fig. 1, last row).

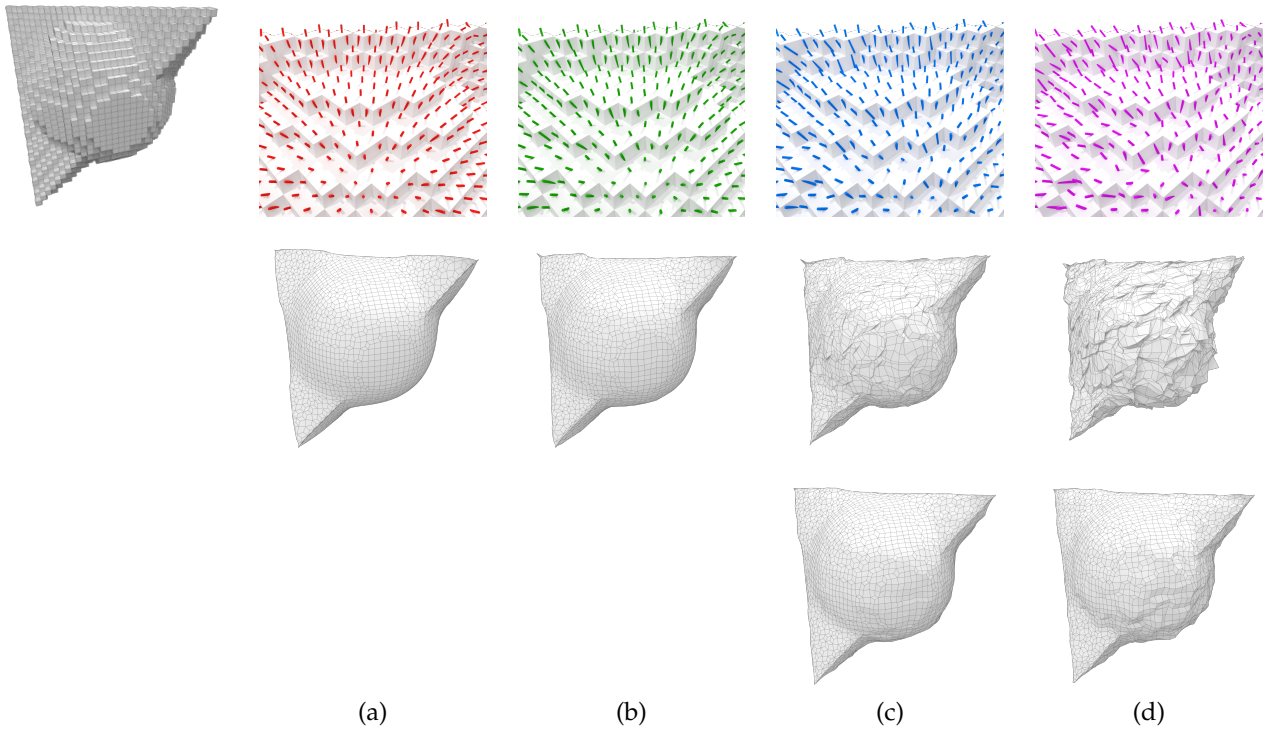

Fig. 1. Stability with respect to noise in the input normal vector field (40^3 shape, same α, β and γ parameters): (a) the regularization with the input normal vector field from [4], (b) random shifts ϵ with $\|\epsilon\| < 0.2$ (up to 11°), (c) with $\|\epsilon\| < 0.5$ (up to 26.5°), and (d) with $\|\epsilon\| < 0.8$ (up to 38.7°). For the second row, we have used the default parameters ($\alpha = 10^{-3}$, $\beta = 1$, $\gamma = 10^{-1}$). For the third row, we have reduced the alignment term ($\beta = 10^{-1}$) to handle the strong noise (only for (c) and (d)).

On the same binary shape, we have performed several regularizations with various input normal vector field estimators in Figure 2. We have tested and compared the results obtained with: (a) a trivial estimator (unit vectors perpendicular to the isothetic input quads), (b) the estimator described in [5] based in Integral Invariants, and two anisotropic estimators: (c) [6] and (d) [4]. Since the last two ones [4], [6] preserve sharp features in the normal field, these features are clearly visible in the corresponding regularizations.

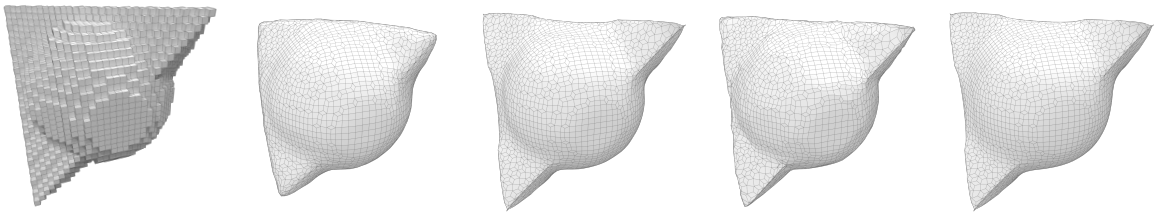

Fig. 2. Regularization for various normal vector estimators: (a) trivial normal vectors, (b) isotropic integral invariant estimator [5], (c) robust anisotropic voting based normal vectors [6], and (d) piecewise smooth anisotropic normal vectors [4].

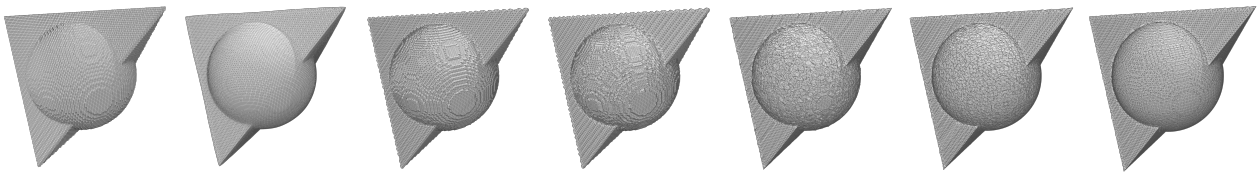

(a) (b) (c) (d) (e) (f) (g)

Fig. 3. From an input shape (a), (b) first presents our regularization. From (c) to (g), we have considered DC for different quantification of the implicit function with 1, 2, 4, 6 and 8 bits.

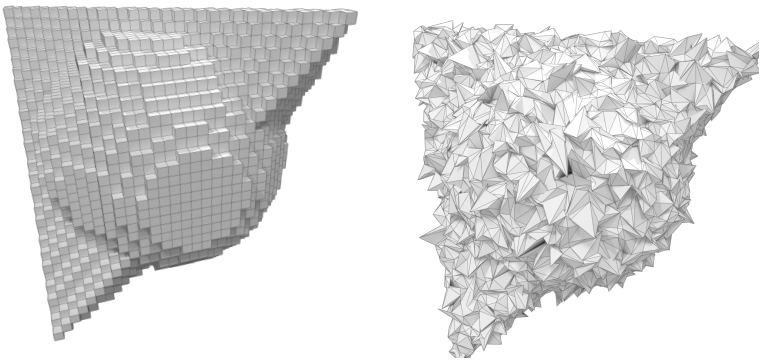

(a) (b)

Fig. 4. Numerical instability of DC when using a robust normal vector field from [4] (same as the one in Fig. 2-(d)) but with positions still located in between adjacent voxels.

To complete the Dual-Contouring discussion, Figure 3 presents DC reconstructions for several quantification steps: the original shape (Fig. 3-(a)) corresponds to a threshold of an implicit function. In Fig. 3-(b), we have the result of our regularization. In Figures (c) to (g) we present the DC surfaces obtained from positions and normal vectors given by several quantification steps of the implicit function (from 1-bit to 8-bits). The 1-bit quantification (c) corresponds to normal vectors given by gradient of the binary image and positions are in between inside/outside voxels. The 8-bits quantification (g) corresponds to normal vectors computed from the gradient of an 8-bits representation of the function. For fine quantification ((f) or (g)), the quality of surfaces increases as we get closer to a pure Hermite data input. However, coarse quantification generates surfaces close to trivial MC surfaces. If we now consider DC with a robust normal vector field (*e.g.* from [4]) but positions $\{\mathbf{s}_j\}$ in between two heterogeneous voxels, we obtain a highly distorted reconstruction (see Fig. 4). Except in the case of almost perfect implicit function iso-contouring, DC produces highly irregular surfaces because of the instability of the local QEF approach.

3 l_2-PROXIMITY AND STABILITY OF THE REGULARIZED SURFACE (PROOF OF PROPOSITION 1)

Assuming that our digital shape X_h was the digitization of some smooth shape $\mathcal{X}$ with a grid sampling step h, we prove here that our regularized surface P^* is close to the boundary of X_h (i.e. the input voxel data) and also close to the underlying unknown continuous surface $\partial\mathcal{X}$. More formally, we have:

Proposition 1 (Proximity and stability)**.** *Let P be the n input voxel vertices of the boundary of X_h, and let P^* be the n output vertices of our regularization process (recall that the input surface and the regularized surface have the same combinatorial structure, so P and P^* are indexed similarly). Then the average distance between P^* and P is upper-bounded by $O(h)$. Furthermore, the same holds between P^* and $\partial\mathcal{X}$. More precisely,*

$$\frac{1}{n}\,\|\mathbf{p}_i^* - \mathbf{p}_i\| \leq C\cdot h\,, \qquad \frac{1}{n}\,d(\mathbf{p}_i^*, \partial\mathcal{X}) \leq C'\cdot h\,, \tag{1}$$

for some constants C, C' that depend uniquely on the reach of $\partial\mathcal{X}$.

A remarkable aspect of this result is that it does not depend on the quality of the input normal vector field. It means that the regularization is very stable in terms of vertex position, while aligning edges as good as possible so that they are orthogonal to the input normal vector field. In practice and as illustrated by experiments, the better is the normal estimator, the closer is P^* to $\partial\mathcal{X}$. Since we use convergent normal estimators like the one of [5] or [4], this explains the quality of the regularization.

The key ingredients to the proof are :

- the fact that ∂X_h and $\partial\mathcal{X}$ are Hausdorff-close in $O(h)$ (see Lemma 1);
- the fact that the projection $\tilde{P}$ of P onto $\partial\mathcal{X}$ has an energy no greater than some constant;
- the fact that P^* has an energy lower than the previous one.
- the fact that convergent normal estimators induce an alignment energy even smaller than data attachment;

We now proceed proving Proposition 1 in detail. In the following, let $\mathcal{X}$ be a compact domain of $\mathbb{R}^3$ with smooth boundary and let X_h be its digitization on a grid with grid-step h (i.e. $X_h = \mathcal{X} \cap (h\mathbb{Z})^3$). Equivalently, the digital set X_h can be represented as a union of cubes of edge length h, i.e. a set of voxels in space. We further denote by ∂X_h the topological boundary of X_h if seen as a union of voxels. It is thus a two-dimensional surface made of squares of side h.

Last, we assume w.l.o.g that the input normal vector field $\mathbf{n}_f$ per face f of $\partial\mathcal{X}_h$ is not too far away from the continuous normal vector field $\mathbf{n}$ of ∂X. More precisely, there is some real number $\delta \in [0,1]$ such that:

$$\forall f \in \partial X_h\,, \forall \mathbf{x} \in X \text{ such that } d(\mathbf{x}-f) \leq h \text{ then } \|\mathbf{n}_f - \mathbf{n}(\mathbf{x})\| \leq O(h^\delta)\,, \tag{2}$$

with $d(\mathbf{x}, f)$ the Euclidean distance between $\mathbf{x}$ and the face f. Note that if $\delta = 0$, the equation above always hold since normal vectors are unitary. In this case, it just means that we do not require any constraint on the input normal vector field. In practice, we use convergent normal estimators. For instance, the one proposed in [5], [7] achieves $\delta = \frac{2}{3}$.

3.1 Digital boundary ∂X_h and continuous boundary $\partial\mathcal{X}$ are geometrically close

This is due to a more general result in [8], whose formulation in 3D is:

Lemma 1 ([8], Theorem 1)**.** *If the reach of $\partial\mathcal{X}$ is greater than R, then, for any digitization step $0 < h < 2R/\sqrt{3}$, the Hausdorff distance between sets $\partial\mathcal{X}$ and ∂X_h is less than $\sqrt{3}h/2$. More precisely:*

$$\forall \mathbf{x} \in \partial\mathcal{X}, \exists \mathbf{y} \in \partial X_h, ||\mathbf{x}-\mathbf{y}|| \leq \frac{\sqrt{3}}{2}h \text{ and } \xi(\mathbf{y}) = \mathbf{x}\,, \tag{3}$$

$$\forall \mathbf{y} \in \partial X_h, ||\mathbf{y}-\xi(\mathbf{y})|| \leq \frac{\sqrt{3}}{2}h\,, \tag{4}$$

where $\xi(\mathbf{y})$ is the projection of $\mathbf{y}$ to the closest point on $\partial\mathcal{X}$ (defined for any point $\mathbf{y} \in \mathbb{R}^3 \setminus MA(\partial\mathcal{X})$, $MA(\partial\mathcal{X})$ being the medial axis of $\mathcal{X}$).

From this lemma, we have that ∂X_h is $\frac{\sqrt{3}}{2}h-$Hausdorff close to $\partial\mathcal{X}$.

3.2 The projection $\tilde{P}$ of P onto ∂X has an energy at most constant

To simplify the presentation, we denote by P (resp. F) the vertices (resp. faces) of ∂X_h. Let us recall the energy of a quadrangulation $\hat{P}$ with the same topological structure as ∂X_h:

$$\mathcal{E}(\hat{P}) = \alpha \sum_{i=1}^{n} \|\mathbf{p}_i - \hat{\mathbf{p}}_i\|^2 + \beta \sum_{f\in F} \sum_{\mathbf{d}\,\hat{\mathbf{p}}\in\partial f} (\mathbf{d}\,\hat{\mathbf{p}} \cdot \mathbf{n}_f)^2 + \gamma \sum_{i=1}^{n} \|\hat{\mathbf{p}}_i - \hat{\mathbf{b}}_i\|^2\,. \tag{5}$$

We let P^* denote the optimal solution minimizing (5). We prove that $\mathcal{E}(P^*)$ has an energy no greater than some $O(1)$. To do so, we examine a particular solution $\tilde{P}$, defined as the projection of P onto $\partial\mathcal{X}$, i.e. $\tilde{P} := \xi(P)$ if ξ is the projection onto $\partial\mathcal{X}$.

The key point is to evaluate the alignment term of the energy for $\tilde{P}$. Hence, we focus first on

$$\beta \sum_{f\in F} \sum_{\mathbf{d}\,\tilde{\mathbf{p}}\in\partial f} (\mathbf{d}\,\hat{\mathbf{p}} \cdot \mathbf{n}_f)^2\,.$$

For a given surfel f of centroid $\dot{f}$, letting $c := \xi(\dot{f})$ being its projection onto $\partial\mathcal{X}$, and a given incident edge $\mathbf{d}\,\tilde{\mathbf{p}} := (\tilde{\mathbf{p}}_1, \tilde{\mathbf{p}}_2) = (\xi(\mathbf{p}_1), \xi(\mathbf{p}_2))$, we have

$$(\mathbf{d}\,\tilde{\mathbf{p}} \cdot \mathbf{n}_f)^2 = (\mathbf{d}\,\tilde{\mathbf{p}} \cdot (\mathbf{n}(c) + \epsilon(f)))^2\,,$$

where $\mathbf{n}(c)$ is the normal vector to $\partial\mathcal{X}$ at c, the projection of the centroid of face f and $\epsilon(f) := (\mathbf{n}_f - \mathbf{n}(c))$, the error in the normal estimation. See Figure 5 for an illustration of the notations.

We decompose the right-hand side into three terms as follows:

$$(\mathbf{d}\,\tilde{\mathbf{p}} \cdot \mathbf{n}_f)^2 = \underbrace{(\mathbf{d}\,\tilde{\mathbf{p}} \cdot \mathbf{n}(c))^2}_{A} + \underbrace{2(\mathbf{d}\,\tilde{\mathbf{p}} \cdot \mathbf{n}(c))(\mathbf{d}\,\tilde{\mathbf{p}} \cdot \epsilon(f))}_{B} + \underbrace{(\mathbf{d}\,\tilde{\mathbf{p}} \cdot \epsilon(f))^2}_{C} \tag{6}$$

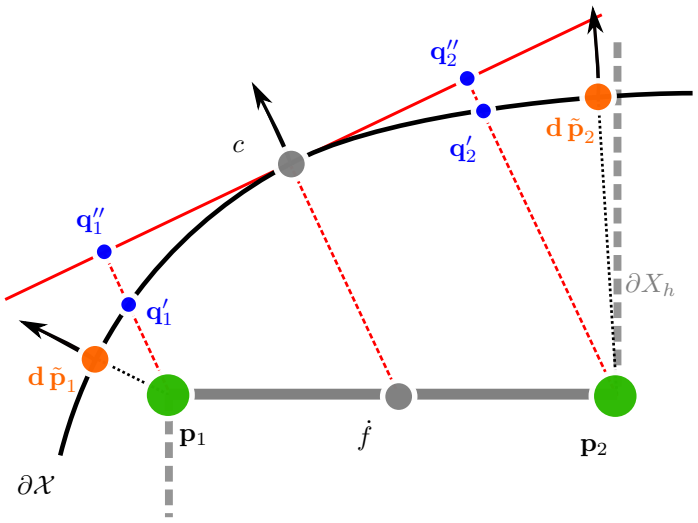

Fig. 5. Illustration of the notations used in the proof of Lemma 1.

First, we have

$$\|\mathbf{d}\,\tilde{\mathbf{p}}\| = \|\tilde{\mathbf{p}}_1 - \tilde{\mathbf{p}}_2\| \leq \|\tilde{\mathbf{p}}_1 - \mathbf{p}_2\| + \|\mathbf{p}_1 - \mathbf{p}_2\| + \|\mathbf{p}_2 - \tilde{\mathbf{p}}_2\| \tag{7}$$

$$\leq \frac{\sqrt{3}}{2}h + h + \frac{\sqrt{3}}{2}h \quad \text{(using Thm. 1)} \tag{8}$$

$$\leq C_1 \cdot h \quad \text{(setting } C_1 := (\sqrt{3}+1)h\text{)}\,. \tag{9}$$

From (2) and (4), we have that $\|\epsilon(f)\| \leq C_2 h^\delta$. With (9), term C of (6) is thus upper-bounded by $C_1^2 C_2^2 \cdot h^{2+2\delta}$.

For terms A and B, we need to develop the expression:

$$\begin{aligned}\mathbf{d}\,\tilde{\mathbf{p}} \cdot \mathbf{n}(c) &= (\tilde{\mathbf{p}}_1 - \tilde{\mathbf{p}}_2) \cdot \mathbf{n}(c) \\ &= ((\mathbf{q}'_1 - \tilde{\mathbf{p}}_1) + (\mathbf{q}''_1 - \mathbf{q}'_1) + (\mathbf{q}''_2 - \mathbf{q}''_1) + (\mathbf{q}'_2 - \mathbf{q}''_2) + (\tilde{\mathbf{p}}_2 - \mathbf{q}'_2)) \cdot \mathbf{n}(c)\,,\end{aligned}$$

with notations illustrated in Figure 5. For short, $\tilde{\mathbf{p}}_i$ and $\mathbf{q}'_i$ are on $\partial\mathcal{X}$, and $\mathbf{q}'_i$ corresponds to the projection of $\mathbf{p}_i$ onto $\partial\mathcal{X}$ along direction $\mathbf{n}(c)$. Furthermore, $\mathbf{q}''_i$ belongs belong to the tangent plane of $\partial\mathcal{X}$ at c.

By construction, $(\mathbf{q}''_2 - \mathbf{q}''_1) \cdot \mathbf{n}(c)) = 0$. Furthermore, we have $(\mathbf{q}''_i - \mathbf{q}'_i) \cdot \mathbf{n}(c) = \pm\|\mathbf{q}''_i - \mathbf{q}'_i\|$ ($\mathbf{n}(c)$ being unitary). Hence,

$$\mathbf{d}\,\tilde{\mathbf{p}} \cdot \mathbf{n}(c) = (\mathbf{q}'_1 - \tilde{\mathbf{p}}_1) \cdot \mathbf{n}(c) \pm \|\mathbf{q}''_1 - \mathbf{q}'_1\| \pm \|\mathbf{q}'_2 - \mathbf{q}''_2\| + (\tilde{\mathbf{p}}_2 - \mathbf{q}'_2) \cdot \mathbf{n}(c)\,. \tag{10}$$

Since $\partial\mathcal{X}$ has positive reach greater than R, the maximal absolute curvature at $\partial\mathcal{X}$ is upper-bounded by $\frac{1}{R}$. For the analysis, the greatest deformation is thus achieved by an approximation of $\partial\mathcal{X}$ by a circle with radius R. Classical geometry on the circle allows us to write, for $h \leq R$:

$$\|\mathbf{q}''_i - \mathbf{q}'_i\| \leq \frac{1}{R}\|\mathbf{q}''_i - c\|^2 \leq \frac{h^2}{4R}\,. \tag{11}$$

We now bound $(\mathbf{q}'_i - \tilde{\mathbf{p}}_i)$. First, using (3)and (4), we observe that

$$\begin{aligned}\|\tilde{\mathbf{p}}_i - c\| &\leq \|\tilde{\mathbf{p}}_i - \mathbf{p}_i\| + \|\mathbf{p}_i - \dot{f}\| + \|\dot{f} - c\| \\ &\leq \frac{\sqrt{3}}{2}h + \frac{h}{2} + \frac{\sqrt{3}}{2}h = (\sqrt{3} + \frac{1}{2})h\,.\end{aligned} \tag{12}$$

Then, we use another result from [8], which states that the map $\mathbf{n}(\cdot)$ is $(\sqrt{3}/R)$-Lipschitz. In other words,

$$\begin{aligned}\|\mathbf{n}(\tilde{\mathbf{p}}_i) - \mathbf{n}(c)\| &\leq \frac{\sqrt{3}}{R}\|\tilde{\mathbf{p}}_i - c\| \\ &\leq \left(3 + \frac{\sqrt{3}}{2}\right)\frac{h}{R} \qquad \text{(using (12))}.\end{aligned} \tag{13}$$

If α is the angle between $\mathbf{n}(\tilde{\mathbf{p}}_i)$ and $\mathbf{n}(c)$,

$$\|\mathbf{q}'_i - \tilde{\mathbf{p}}_i\| \leq \sin(\alpha) \cdot \max(\|\mathbf{p}_i - \tilde{\mathbf{p}}_i\|, \|\mathbf{q}'_i - \mathbf{p}_i\|)\,. \tag{14}$$

We know that $\|\mathbf{p}_i - \tilde{\mathbf{p}}_i\| \leq \frac{\sqrt{3}}{2}h$. To estimate $\|\mathbf{q}'_i - \mathbf{p}_i\|$, we perform the following decomposition

$$\begin{aligned}\|\mathbf{q}'_i - \mathbf{p}_i\| &\leq \|\mathbf{p}_i - f\| + \|f - c\| + \|c - \mathbf{q}''_i\| + \|\mathbf{q}'_i - \mathbf{q}''_i\| \\ &\leq \frac{h}{2} + \frac{\sqrt{3}}{2}h + \frac{h}{2} + \frac{h^2}{4R} \qquad \text{(using (11) for the last term)} \\ &\leq \left(1 + \frac{\sqrt{3}}{2} + \frac{1}{4}\right) h \qquad \text{(for } h \leq R\text{)}. \end{aligned} \tag{15}$$

Note that (15) is larger than $\frac{\sqrt{3}}{2}h$ for the $\max(\cdot,\cdot)$ term in (14). Since $\frac{\sin(\alpha)}{\pi} \leq \frac{\alpha}{\pi} \leq \sin(\frac{\alpha}{2})$ for positive angles lesser than $\pi/2$, we bound $\sin(\alpha)$ with:

$$\sin(\alpha) \leq \frac{\pi}{2}\|\mathbf{n}(\tilde{\mathbf{p}}_i) - \mathbf{n}(c)\| \leq \frac{\pi}{2}\left(3 + \frac{\sqrt{3}}{2}\right)\frac{h}{R}. \tag{16}$$

Using (15) and (16) into (14), we conclude

$$\begin{aligned}\|\mathbf{q}'_i - \tilde{\mathbf{p}}_i\| &\leq \left(1 + \frac{\sqrt{3}}{2} + \frac{1}{4}\right)\frac{\pi}{2}\left(3 + \frac{\sqrt{3}}{2}\right)\frac{h^2}{R} \\ &\leq C_3 \cdot h^2\,. \end{aligned} \tag{17}$$

Using (11) and (17), (10) becomes

$$\begin{aligned}\mathbf{d}\,\tilde{\mathbf{p}} \cdot \mathbf{n}(c) &\leq (\mathbf{q}'_1 - \tilde{\mathbf{p}}_1) \cdot \mathbf{n}(c) + \|\mathbf{q}''_1 - \mathbf{q}'_1\| + \|\mathbf{q}'_2 - \mathbf{q}''_2\| + (\tilde{\mathbf{p}}_2 - \mathbf{q}'_2) \cdot \mathbf{n}(c) \\ &\leq 2C_3 \cdot h^2 + \frac{h^2}{2R} \\ &\leq C_4 \cdot h^2\,. \end{aligned}$$

Putting everything together, we rewrite (6) as

$$\begin{aligned}(\mathbf{d}\,\tilde{\mathbf{p}} \cdot \mathbf{n}_f)^2 &= (\mathbf{d}\,\tilde{\mathbf{p}} \cdot \mathbf{n}(c))^2 + 2(\mathbf{d}\,\tilde{\mathbf{p}} \cdot \mathbf{n}(c))(\mathbf{d}\,\tilde{\mathbf{p}} \cdot \epsilon(f)) + (\mathbf{d}\,\tilde{\mathbf{p}} \cdot \epsilon(f))^2 \\ &\leq C_4^2 h^4 + 2(C_4^2 \cdot h^2) \cdot ((C_1 \cdot h) \cdot (C_2 \cdot h^\delta)) + C_1^2 C_2^2 \cdot h^{2+2\delta} \\ &\leq K \cdot h^{2+2\delta}, \end{aligned} \tag{18}$$

where constant K depends only on R.

We bound now the third term (fairness term), where locally we have to bound $\|\tilde{\mathbf{p}}_i - \tilde{\mathbf{b}}_i\|$:

$$\begin{aligned}\|\tilde{\mathbf{p}}_i - \tilde{\mathbf{b}}_i\| &= \|\tilde{\mathbf{p}}_i - \frac{1}{|N(i)|}\sum_{j \in N(i)} \tilde{\mathbf{p}}_j\| && \text{(where } N(i) \text{ are the neighbors of vertex } i\text{)} \\ &\leq \frac{1}{|N(i)|}\sum_{j \in N(i)} \|\tilde{\mathbf{p}}_i - \tilde{\mathbf{p}}_j\| && \text{(using triangular inequality)} \\ &\leq \frac{1}{|N(i)|}\sum_{j \in N(i)} \|\tilde{\mathbf{p}}_i - \mathbf{p}_i\| + \|\mathbf{p}_i - \mathbf{p}_j\| + \|\mathbf{p}_j - \tilde{\mathbf{p}}_j\| && \text{(using triangular inequality)} \\ &\leq \frac{1}{|N(i)|}\sum_{j \in N(i)} \left(\frac{\sqrt{3}}{2}h + h + \frac{\sqrt{3}}{2}h\right) && \text{(using (4))} \\ &\leq (1 + \sqrt{3})h && \text{(simplifying the expression).} \end{aligned} \tag{19}$$

We can now give the energy of $\tilde{P}$ bounding the contribution of each edge to the energy

$$\begin{aligned}\mathcal{E}(\tilde{P}) &= \alpha\sum_{i=1}^{n}\|\mathbf{p}_i - \tilde{\mathbf{p}}_i\|^2 + \beta\sum_{f \in F}\sum_{\mathbf{d}\,\tilde{\mathbf{p}} \in \partial f}(\mathbf{d}\,\tilde{\mathbf{p}} \cdot \mathbf{n}_f)^2 + \gamma\sum_{i=1}^{n}\|\tilde{\mathbf{p}}_i - \tilde{\mathbf{b}}_i\|^2 \\ &\leq \alpha n\frac{3}{4}h^2 + \beta\sum_{f \in F}\sum_{\mathbf{d}\,\tilde{\mathbf{p}} \in \partial f}(\mathbf{d}\,\tilde{\mathbf{p}} \cdot \mathbf{n}_f)^2 + \gamma n(1 + \sqrt{3})^2 h^2 && \text{(using (4) and (19))} \\ &\leq \alpha n\frac{3}{4}h^2 + 4\beta m K \cdot h^{2+2\delta} + \gamma n(1 + \sqrt{3})^2 h^2 && \text{(using (18))} \end{aligned} \tag{20}$$

For a smooth shape $\partial\mathcal{X}$ with positive reach, we bound the number of vertices n and faces m of ∂X_h by $O(h^{-2})$ (e.g. see [8], immediate consequence of Lemma 10). As a consequence, we conclude that $\mathcal{E}(\tilde{P})$ is in $O(1)$ as h tends to zero, whatever is the value of $\delta \geq 0$.

3.3 Proximity of P^* to P and to $\partial\mathcal{X}$

The rest of the proof is more straightforward. First, since P^* is a minimizer of the energy and using the bound above, we have

$$\mathcal{E}(P^*) \leq \mathcal{E}(\tilde{P}) = O(1) \tag{21}$$

As a consequence, if we decompose $\mathcal{E}(P^*)$, we have

$$\alpha \sum_{i=1}^{n} \|\mathbf{p}_i - \mathbf{p}_i^*\|^2 + \beta \sum_{f \in F} \sum_{\mathbf{d}\,\mathbf{p}^* \in \partial f} (\mathbf{d}\,\mathbf{p}^* \cdot \mathbf{n}_f)^2 + \gamma \sum_{i=1}^{n} \|\mathbf{p}_i^* - \mathbf{b}_i^*\|^2 \leq K' \tag{22}$$

for some constant K' in the $O(1)$ bound of (21). Eq. (22) being a sum of three positive terms, we have

$$\alpha \sum_{i=1}^{n} \|\mathbf{p}_i - \mathbf{p}_i^*\|^2 \leq K' \,.$$

Using Cauchy-Schwartz inequality, we have

$$\sum_{i=1}^{n} \|\mathbf{p}_i - \mathbf{p}_i^*\| \leq \left(\sum_{i=1}^{n} \|\mathbf{p}_i - \mathbf{p}_i^*\|^2 \right)^{1/2} \sqrt{n} \,.$$

Finally, the average error as stated in Proposition 1 can be rewritten as

$$\frac{\sum_{i=1}^{n} \|\mathbf{p}_i - \mathbf{p}_i^*\|}{n} = \sqrt{\frac{K'}{\alpha}} \frac{1}{\sqrt{n}} \,. \tag{23}$$

Since the orthogonal projection ξ of ∂X_h onto $\partial\mathcal{X}$ is surjective and the Jacobian is upperbounded by 4 ([8], Lemma 9), we have $\text{Area}(\partial\mathcal{X}) = \text{Area}(\xi(\partial X_h)) \leq 4\text{Area}(\partial X_h) = 4mh^2$, with m the number of faces of ∂X_h, each of area h^2. Since $n = \Theta(m)$, we have $n = \Omega(1/h^2)$. So $1/\sqrt{n} = O(h)$ and thus

$$\frac{\sum_{i=1}^{n} \|\mathbf{p}_i - \mathbf{p}_i^*\|}{n} = O(h) \,, \tag{24}$$

which concludes the left bound in (1) of Proposition 1. The right bound is an immediate consequence of the fact that the digital surface P is itself $O(h)-$Hausdorff close to $\partial\mathcal{X}$ (see Lemma 1).

3.4 Impact of the input normal vector field

As seen above, the regularized surface is always close to the continuous shape boundary $\partial\mathcal{X}$, with a distance in $O(h)$ on average. This is even true for bad normal estimations. Of course, the better the normal estimation, the nicer the regularized surface. This can be seen in (20). Indeed, if parameter α is set small with respect to β (which is our case in all experiments), then the energy of the projection $\xi(P)$ decreases in $O(h^{2\delta})$. Choosing convergent normal estimators like in [5], [7] implies $\delta = \frac{2}{3}$. So this energy characterizing normal alignment decreases quickly to 0 as h tends to 0. Since the optimal solution P^* has an even smaller energy than $\xi(P)$, it means that P^* has almost the same normal vector field as $\partial\mathcal{X}$, while being close on average. Otherwise said, it is almost the same surface. This explains why the regularized surface looks so much as the boundary of the underlying continuous shape.

4 Gradient of $\mathcal{E}$ as a linear operator

In this section, we briefly describe the construction of the sparse linear system obtained from the equation $\nabla\mathcal{E}(\mathbf{p}^*) = \mathbf{0}$ as proposed in [9].

Let $\mathbf{p}$ (resp. $\hat{\mathbf{p}}$) be the $3n$ column vector constructed by packing all n initial vertices coordinates together (resp. all n regularized vertices coordinates together). The norm used in the data attachment term can be defined from some scalar product on $\mathbb{R}^{3n}$ defined by a $3n \times 3n$ SDP matrix $\bar{\mathbf{W}}_0$. The data attachment energy can then be expressed as

$$\sum_{i=1}^{n} \|\mathbf{p}_i - \hat{\mathbf{p}}_i\|^2 = (\mathbf{p} - \hat{\mathbf{p}})^T \bar{\mathbf{W}}_0 (\mathbf{p} - \hat{\mathbf{p}}) \,. \tag{25}$$

The definition of the barycenter appearing in the fairness term

$$\hat{\mathbf{b}}_i := \frac{1}{|N(i)|} \sum_{j \in N(i)} \hat{\mathbf{p}}_j$$

is linear with respect to $\hat{\mathbf{p}}$. Hence, there exists a $3n \times 3n$ sparse matrix $\mathbf{B}$ such that $\hat{\mathbf{b}} = \mathbf{B}\,\hat{\mathbf{p}}$. Using the same scalar product as before, we can express the fairness energy as

$$\sum_{i=1}^{n} \|\hat{\mathbf{p}}_i - \hat{\mathbf{b}}_i\|^2 = \hat{\mathbf{p}}^T (\mathbf{I} - \mathbf{B})^T \bar{\mathbf{W}}_0 (\mathbf{I} - \mathbf{B}) \hat{\mathbf{p}} \tag{26}$$

where $\mathbf{I}$ the $3n \times 3n$ identity matrix.

Let p be the number of edges of P and recall that m is its number of faces. We can define a $3p \times 3n$ sparse matrix $\mathbf{D}$ which represents edges from vertices positions, that is $\mathbf{d}\,\hat{\mathbf{p}} = \mathbf{D}\,\hat{\mathbf{p}}$. Another $4m \times 3p$ sparse matrix $\mathbf{U}$ can be built to compute, for each faces, the scalar product between the prescribed face normal vector and the four edges vectors. Introducing finally a $4m \times 4m$ SDP matrix $\bar{\mathbf{W}}_2$ linked to a scalar product in $\mathbb{R}^{4m}$, we can express the normal alignment energy as

$$\sum_{f \in F} \sum_{\mathbf{d}\,\hat{\mathbf{p}}_j \in \partial f} (\mathbf{d}\,\hat{\mathbf{p}}_j \cdot \mathbf{n}_f)^2 = \hat{\mathbf{p}}^T\,\mathbf{D}^T\,\mathbf{U}^T\,\bar{\mathbf{W}}_2\,\mathbf{U}\,\mathbf{D}\,\hat{\mathbf{p}} \tag{27}$$

Now $\mathcal{E}(\hat{\mathbf{p}})$ has a fully matricial expression and its gradient with respect to $\hat{\mathbf{p}}$ can be computed using quadratic form matrix differentiation. This lead to the following expression for $\nabla\mathcal{E}(\mathbf{p}^*) = \mathbf{0}$

$$\Big(\alpha\bar{\mathbf{W}}_0 + \beta\,\mathbf{D}^T\,\mathbf{U}^T\,\bar{\mathbf{W}}_2\,\mathbf{U}\,\mathbf{D} + \gamma(\mathbf{I}-\mathbf{B})^T\bar{\mathbf{W}}_0(\mathbf{I}-\mathbf{B})\Big)\,\hat{\mathbf{p}} = \alpha\bar{\mathbf{W}}_0\mathbf{p}\,. \tag{28}$$

Note that this linear system is sparse if the scalar product matrices $\bar{\mathbf{W}}_0$ and $\bar{\mathbf{W}}_2$ are sparse, that is if spatially localized scalar products are used. Furthermore, as long as weights α, β and γ are positive (and strictly positive for α), the linear operator on the left-hand side of (28) is positive definite and thus invertible.

REFERENCES

[1] G. M. Nielson, G. Graf, R. Holmes, A. Huang, and M. Phielipp, "Shrouds: Optimal separating surfaces for enumerated volumes," in *VisSym*, vol. 3, 2003, pp. 75–84.

[2] G. T. Herman, "Discrete multidimensional jordan surfaces," *CVGIP: Graphical Models and Image Processing*, vol. 54, no. 6, pp. 507–515, 1992.

[3] J.-O. Lachaud and A. Montanvert, "Continuous analogs of digital boundaries: A topological approach to iso-surfaces," *Graphical models*, vol. 62, no. 3, pp. 129–164, 2000.

[4] D. Coeurjolly, M. Foare, P. Gueth, and J.-O. Lachaud, "Piecewise smooth reconstruction of normal vector field on digital data," *Computer Graphics Forum, Pacific Graphics 2016 Proceedings*, Proc. Pacific Graphics 2016, vol. 35, no. 7, Sep. 2016.

[5] D. Coeurjolly, J.-O. Lachaud, and J. Levallois, "Multigrid Convergent Principal Curvature Estimators in Digital Geometry," en, *Computer Vision and Image Understanding*, vol. 129, no. 1, pp. 27–41, Jun. 2014.

[6] A. Boulch and R. Marlet, "Fast and robust normal estimation for point clouds with sharp features," *Computer Graphics Forum*, vol. 31, no. 5, pp. 1765–1774, 2012.

[7] J.-O. Lachaud, D. Coeurjolly, and J. Levallois, "Robust and Convergent Curvature and Normal Estimators with Digital Integral Invariants," in *Modern Approaches to Discrete Curvature*, ser. Lecture Notes in Mathematics, P. R. Laurent Najman, Ed., vol. 2184, Springer-Verlag, 2017.

[8] J.-O. Lachaud and B. Thibert, "Properties of gauss digitized shapes and digital surface integration," *Journal of Mathematical Imaging and Vision*, vol. 54, no. 2, pp. 162–180, 2016.

[9] D. Coeurjolly, P. Gueth, and J.-O. Lachaud, "Digital surface regularization by normal vector field alignment," in *20th International Conference on Discrete Geometry for Computer Imagery*, ser. 20th International Conference on Discrete Geometry for Computer Imagery, vol. LNCS, Vienna, Austria, 2017.